

Identifiability of generalised Randles circuit models

S.M.Mahdi Alavi, Adam Mahdi, Stephen J. Payne and David A. Howey

Abstract—The Randles circuit (including a parallel resistor and capacitor in series with another resistor) and its generalised topology have widely been employed in electrochemical energy storage systems such as batteries, fuel cells and supercapacitors, also in biomedical engineering, for example, to model the electrode-tissue interface in electroencephalography and baroreceptor dynamics. This paper studies identifiability of generalised Randles circuit models, that is, whether the model parameters can be estimated uniquely from the input-output data. It is shown that generalised Randles circuit models are structurally locally identifiable. The condition that makes the model structure globally identifiable is then discussed. Finally, the estimation accuracy with respect to noise-free, noisy, zero- and nonzero- mean data is evaluated through extensive simulations. The existing trade-off between the estimation of Warburg term and other parameters by using zero- and nonzero- mean data is fully discussed.

Index Terms—Randles circuit, Identifiability, System identification, Parameter estimation.

I. INTRODUCTION

Randles proposed an equivalent circuit for the kinetics of rapid electrode reactions in [1]. Since then, the model has been developed and has become the basis for the study of many electrochemical energy storage systems such as batteries, fuel cells and supercapacitors, [2], [3]. Figure 1 shows a generalised Randles model consisting of an ohmic resistor, R_∞ , in series with a number of parallel resistors and capacitors, and a capacitor C_w . In electrochemical applications, the ohmic resistor R_∞ represents usually the conduction of charge carriers through electrolyte and metallic conductors. The resistors and capacitors in the parallel pairs represent the charge transfer resistance and the double layer capacitance, respectively, or are an approximation of a diffusion process, [4], [5]. The number of parallel R 's and C 's depends on how many of these pairs are required such that the frequency response of the generalised Randles model fits with the device impedance spectra within the frequency range of interests [6]–[8]. For instance, in [8], the number of the parallel pairs was determined by minimising the error between the model and measured voltages. The capacitor C_w , also known as

the Warburg term, accounts for a diffusion process, [4], [5]; or in a battery or supercapacitor, it may represent state of charge [9]. It should be noted that the open-circuit voltage source is not considered in the generalised Randles model Figure 1 and it is only focused on the impedance model in this paper.

The generalised Randles circuit models have also been employed in biomedical engineering. An electric circuit model of the electrode-tissue interface in electroencephalography includes two parallel R-C pairs in series with two resistors and two voltage sources [10], which is a special case of the circuit given in Figure 1. It is noted that C_w can be considered as a parallel R and C with $R = \infty$. The viscoelastic analog of the generalised Randles model is employed in cardiovascular and cerebral haemodynamics modeling, in describing the viscoelastic properties of the aortic wall and the coupling of the nerve endings of the baroreceptor neurons in the carotid sinus and aortic arch [11], [12]; and in relating the fluctuation of the arterial blood pressure with the cerebral blood flow velocity [13].

The identification or parameter estimation of the generalised Randles model (with different numbers of parallel R 's and C 's) is important in condition monitoring, fault diagnosis and control [3], [9], [14]–[20]. In [14], the authors showed that the Randles circuit can be used for monitoring the battery charge transfer overvoltage. In [15], identification tests for parameter estimation of lead-acid batteries are suggested. In [20], identification through fitting the impedance spectra in the frequency domain is presented.

The objective of this paper is to study the identifiability of the generalised Randles model shown in Figure 1, that is, whether the model parameters can be estimated uniquely from input-output data. Typically the identifiability problem is divided into two broad areas: parameter estimation accuracy and structural identifiability. *Parameter estimation accuracy* considers the practical aspects of the problem that come with real data such as noise and bias [21]. In studying *structural identifiability*, on the other hand, one assumes that noise-free informative data is available and therefore it is, in fact, a data-independent concept. Unidentifiable parameters can be assigned an infinite number of values yet still lead to identical input-output data. Thus, structural identifiability is a necessary condition for identifiability and parameter estimation. A number of analytical approaches to structural identifiability have been proposed, including Laplace transform (transfer function) [22], [23], Taylor series expansion [24], [25], similarity transformations [26]–[33], and differential algebra [34], [35]. In linear systems, it has been shown that controllability and observability properties are closely related to the concept of structural identifiability, [30]–

S.M.M. Alavi was with the Energy and Power Group, Department of Engineering Science, University of Oxford. He is now with the Brain Stimulation Engineering Laboratory, Duke University, Durham, NC 27710, USA. Email: mahdi.alavi@duke.edu

A. Mahdi and S.J. Payne are with the Institute of Biomedical Engineering, Department of Engineering Science, University of Oxford, Old Road Campus Research Building, Oxford, OX3 7DQ, United Kingdom. Emails: {adam.mahdi, stephen.payne}@eng.ox.ac.uk

D.A. Howey is with the Energy and Power Group, Department of Engineering Science, University of Oxford, Parks Road, Oxford, OX1 3PJ, United Kingdom. Email: david.howey@eng.ox.ac.uk

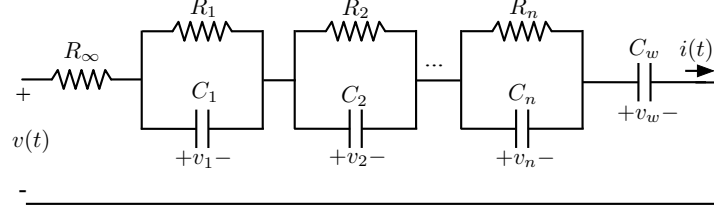


Fig. 1. The generalised Randles equivalent circuit model.

[33]. For example, it was shown that single-input single-output linear time-invariant systems are structurally identifiable if and only if their observer canonical form is controllable (see Chapter 4 in [33]). However, controllable and observable systems can still be unidentifiable in the general case [31].

Recently, there has been a significant interest in the identifiability analysis of battery models [36]–[43]. In [36], the structural identifiability of a five-element equivalent circuit model (ECM) including two capacitors was discussed by comparing the number of unknown parameters of the Transfer Function (TF) and the circuit. In [37], the structural identifiability of a more general nonlinear ECM is analysed based on the observability conditions. It is shown that cells with serial connections are not observable, demonstrating that complete estimation of the state-of-charge and model parameters from lumped measurements with series cells is not possible through independent measurements. However, it is shown that lumped models with parallel connectivities are observable provided that none of the parallel cells are identical. The identifiability of battery electrochemical models was discussed in [38]–[41]. In particular, it was shown that some of the electrochemical model parameters are not identifiable given typical charge-discharge cycles [38]–[40]. In [41], it was shown that the shape of the charge-discharge cycles plays a crucial role in the identifiability of battery parameters. It was also demonstrated that the system identification method can be employed in monitoring the battery film growth. The identifiability problem of Randles ECMs has been studied in [42], [43], where the authors consider models that include up to two capacitors, and the analysis is based on the Fisher information matrix (FIM). The FIM provides some information about the sensitivity of the measurement to the model parameters by using likelihood functions, [44]. In [42], a bound of estimation errors was developed by using the Cramér-Rao theorem. In [43], a method was proposed to optimally shape the battery cycles and improve the identifiability.

This paper shows that the generalised Randles model in Figure 1 is structurally globally identifiable for $n = 1$, and structurally locally identifiable for any finite $n > 1$, and becomes globally identifiable assuming an ordering through the generalised circuit. Finally, the identifiability of the model is assessed through extensive simulations.

II. THE MODEL PARAMETERISATION AND PROBLEM STATEMENT

The state-space and TF parameterised models of the generalised Randles circuit given in Figure 1 are derived.

Define the electric current as the system input $u(t) = i(t) \in \mathbb{R}$, the terminal voltage as the system output $y(t) = v(t) \in \mathbb{R}$, the voltages across the internal R-C pairs as the states $\mathbf{x}(t) = [v_1(t) \ \cdots \ v_n(t) \ v_w(t)]^\top \in \mathbb{R}^{n+1}$, and the model parameters as

$$\boldsymbol{\theta} = [R_\infty \ R_1 \ \cdots \ R_n \ C_1 \ \cdots \ C_n \ C_w], \quad (1)$$

where $\boldsymbol{\theta}$ belongs to some open subset $\mathcal{D} \subset \mathbb{R}^{2n+2}$.

A. State-space parametrisation

By using Kirchhoff's laws, a state-space model structure of the Randles circuit, parameterised by $\boldsymbol{\theta}$, can be written as:

$$\begin{cases} \frac{d}{dt}\mathbf{x}(t) = A(\boldsymbol{\theta})\mathbf{x}(t) + B(\boldsymbol{\theta})u(t) \\ y(t) = C(\boldsymbol{\theta})\mathbf{x}(t) + D(\boldsymbol{\theta})u(t) \end{cases} \quad (2)$$

where $A(\boldsymbol{\theta}) \in \mathbb{R}^{(n+1) \times (n+1)}$, $B(\boldsymbol{\theta}) \in \mathbb{R}^{n+1}$, $C(\boldsymbol{\theta})^\top \in \mathbb{R}^{n+1}$ and $D(\boldsymbol{\theta}) \in \mathbb{R}$ are matrices that depend on the parameter vector $\boldsymbol{\theta}$, and are given by

$$A(\boldsymbol{\theta}) = \begin{bmatrix} -a_1(\boldsymbol{\theta}) & 0 & \cdots & 0 & 0 \\ 0 & -a_2(\boldsymbol{\theta}) & \cdots & 0 & 0 \\ \vdots & \vdots & \ddots & \vdots & \vdots \\ 0 & 0 & \cdots & -a_n(\boldsymbol{\theta}) & 0 \\ 0 & 0 & \cdots & 0 & 0 \end{bmatrix}, \quad B(\boldsymbol{\theta}) = \begin{bmatrix} b_1(\boldsymbol{\theta}) \\ b_2(\boldsymbol{\theta}) \\ \vdots \\ b_n(\boldsymbol{\theta}) \\ b_w(\boldsymbol{\theta}) \end{bmatrix}, \quad C(\boldsymbol{\theta})^\top = \begin{bmatrix} 1 \\ 1 \\ \vdots \\ 1 \\ 1 \end{bmatrix}, \quad D(\boldsymbol{\theta}) = d, \quad (3)$$

with time constants $\tau_i = R_i C_i$ for $i = 1, \dots, n$ and

$$a_i = \frac{1}{\tau_i}, \quad b_i = \frac{1}{C_i}, \quad b_w = \frac{1}{C_w}, \quad d = R_\infty. \quad (4)$$

B. Transfer function parametrisation

Denote the model's TF by $T(s, \boldsymbol{\theta})$, where s represents the Laplace operator. Using the formula $T(s, \boldsymbol{\theta}) = C(sI - A)^{-1}B + D$, a parameterised TF of the generalised Randles

circuit can be written as:

$$T(s, \boldsymbol{\theta}) = \sum_{i=1}^n \frac{b_i(\boldsymbol{\theta})}{s + a_i(\boldsymbol{\theta})} + \frac{b_w(\boldsymbol{\theta})}{s} + D(\boldsymbol{\theta}). \quad (5)$$

C. Problem statement

Determine the conditions for the model structure (5) (equivalently in the state-space form (2) and (3)), where $\boldsymbol{\theta}$ is an unknown parameter vector (1), to be locally and/or globally structurally identifiable.

III. MAIN RESULTS

Following [33] a definition of structural identifiability is given as follows.

Definition 1: Let \mathcal{M} be a model structure with the TF $T(s, \boldsymbol{\theta})$, parametrized by $\boldsymbol{\theta}$, where $\boldsymbol{\theta}$ belongs to an open subset $\mathcal{D}_T \subset \mathbb{R}^m$, and consider the equation

$$T(s, \boldsymbol{\theta}) = T(s, \boldsymbol{\theta}^*) \quad \text{for almost all } s, \quad (6)$$

where $\boldsymbol{\theta}, \boldsymbol{\theta}^* \in \mathcal{D}_T$. Then, the model structure \mathcal{M} is said to be

- *globally identifiable* if (6) has a unique solution in \mathcal{D}_T ,
- *locally identifiable* if (6) has a finite number of solutions in \mathcal{D}_T ,
- *unidentifiable* if (6) has an infinite number of solutions in \mathcal{D}_T .

Remark 1: Instead of Definition 1, one can use the so-called coefficient map defined as follows, [28], [29]. Consider the monic¹ TF:

$$T(s, \boldsymbol{\theta}) = \frac{c_0(\boldsymbol{\theta}) + c_1(\boldsymbol{\theta})s + \dots + c_{k_1}(\boldsymbol{\theta})s^{k_1}}{d_0(\boldsymbol{\theta}) + d_1(\boldsymbol{\theta})s + \dots + d_{k_2-1}(\boldsymbol{\theta})s^{k_2-1} + s^{k_2}}, \quad (7)$$

and associate with it the following *coefficient map* $\mathcal{C}_T : \mathbb{R}^m \supset \mathcal{D}_T \rightarrow \mathbb{R}^{k_1+k_2+1}$ defined as

$$\mathcal{C}_T(\boldsymbol{\theta}) = [c_0(\boldsymbol{\theta}), \dots, c_{k_1}(\boldsymbol{\theta}), d_0(\boldsymbol{\theta}), \dots, d_{k_2-1}(\boldsymbol{\theta})]. \quad (8)$$

The model structure \mathcal{M} is globally identifiable if the coefficient map \mathcal{C}_T is one-to-one (injective); locally identifiable if \mathcal{C}_T is many-to-one; and unidentifiable if it is infinitely many-to-one.

The following lemma will be used in the proof of the identifiability of the generalised Randles circuit model.

Lemma 1: Let $\mathcal{C}_T(m)$ be a coefficient map associated with the TF

$$T(s, \boldsymbol{\theta}) = \sum_{i=1}^m \frac{b_i}{s + a_i} + d,$$

where $\boldsymbol{\theta} = (a_1, \dots, a_m, b_1, \dots, b_m, d)$ and $a_i \in \mathbb{R}$ for $i = 1, \dots, m$ are pairwise different. Then the following statements hold:

- (a) If $m = 1$, then $\mathcal{C}_T(m)$ is one-to-one.
- (b) If $m > 1$, then $\mathcal{C}_T(m)$ is many-to-one.

¹In a monic TF, all coefficients are normalised such that the coefficient of the greatest order in the denominator is 1.

Proof. *Part(a).* For $m = 1$, the identifiability equation (6) is given by

$$\frac{b_1}{s + a_1} + d = \frac{b_1^*}{s + a_1^*} + d^*$$

and has a unique solution $(a_1, b_1, d) = (a_1^*, b_1^*, d^*)$, which proves part (a).

Part(b). For $m > 1$, the identifiability equation (6) is given by

$$\sum_{i=1}^m \frac{b_i}{s + a_i} + d = \sum_{i=1}^m \frac{b_i^*}{s + a_i^*} + d^*. \quad (9)$$

We claim that equation (9) admits only finite (more precisely, $m! = 1 \times 2 \times \dots \times m$) number of solutions. To prove the claim note that (9) is the equality of two rational functions, which is satisfied provided that

$$(s + a_1) \times \dots \times (s + a_m) = (s + a_1^*) \times \dots \times (s + a_m^*). \quad (10)$$

Since m distinct roots uniquely characterise a monic polynomial of degree m , and there are $m!$ permutations of m roots of $(s + a_1) \times \dots \times (s + a_m)$, equation (10) has $m!$ solutions. Now, let us fix the permutation $s : \{1, \dots, m\} \rightarrow \{1, \dots, m\}$ and consider an assignment $(a_1, \dots, a_m) = (a_{s_1}^*, \dots, a_{s_m}^*)$. Since a_i for $i = 1, \dots, m$ are assumed to be pairwise distinct, the expressions $1/(s + a_i)$, thought of as functions of the variable s , are linearly independent. Finally, since each side of equation (9) is a linear combination of linearly independent functions, we immediately obtain that $b_j = b_{s_j}^*$ for $i = 1, \dots, m$. This concludes the proof of part (b). \square

Now, we introduce the concept of reparametrisation (see e.g. [28]), which we will use the proof of our main theorem.

Definition 2: A *reparametrisation* of the model structure \mathcal{M} with the coefficient map \mathcal{C}_T is a map $\mathcal{R} : \mathbb{R}^k \supset \mathcal{D}_T \rightarrow \mathbb{R}^m$ such that

$$\text{Im}(\mathcal{C}_T \circ \mathcal{R}) = \text{Im} \mathcal{C}_T, \quad (11)$$

where Im denotes the image of the map. Moreover, the reparameterisation is identifiable if the map $\mathcal{C}_T \circ \mathcal{R} : \mathbb{R}^k \supset \mathcal{D} \rightarrow \mathbb{R}^{k_1+k_2+1}$ is identifiable.

The main result of this section is the following theorem which describes the identifiability of the generalised Randles circuit.

Theorem 1: Let $\mathcal{M}_{RC}(n)$ denotes the state-space model structure (2) with the matrices (3) parametrised by (4), where n is the number of parallel RC elements connected in series (see Figure 1). Then the following conditions hold:

- (a) If $n = 1$, then the model structure $\mathcal{M}_{RC}(n)$ is globally identifiable.
- (b) If $n > 1$, then the model structure $\mathcal{M}_{RC}(n)$ is locally identifiable.
- (c) If $n > 1$, and there is an ordering through the generalised circuit as

$$a_n < a_{n-1} < \dots < a_1, \quad (12)$$

then the model structure $\mathcal{M}_{RC}(n)$ is globally identifiable.

Proof. Consider the model structure $\mathcal{M}_{RC}(n)$ and let $T(s, \theta)$ denote the corresponding TF given by (5), where the parameter vector θ is given by (1). We write $T(s, \theta)$ as a rational function (7) of degree $k_1 = k_2 = n + 1$ and associate with it the coefficient map $\mathcal{C}'_T : \mathbb{R}^{2n+2} \supset \mathcal{D} \rightarrow \mathbb{R}^{2n+3}$.

Part (a). For $n = 1$, the coefficient map $\mathcal{C}'_T : \mathbb{R}^4 \supset \mathcal{D} \rightarrow \mathbb{R}^5$ can be written explicitly as

$$\mathcal{C}'_T(\theta) = [c_0(\theta), c_1(\theta), c_2(\theta), d_0(\theta), d_1(\theta)],$$

where

$$c_0(\theta) = \frac{1}{R_1 C_1 C_w}, \quad c_1(\theta) = \frac{R_\infty C_w + R_1 C_w + R_1 C_1}{R_1 C_1 C_w},$$

$$c_2(\theta) = R_\infty, \quad d_0(\theta) = 0, \quad d_1(\theta) = \frac{1}{R_1 C_1}.$$

By direct computation, we can check that equation $\mathcal{C}'_T(\theta) = \mathcal{C}'_T(\theta^*)$ admits a unique solution $\theta = \theta^*$. Thus the coefficient map is one-to-one, and the model structure is globally identifiable.

Part (b). For $n > 1$, the coefficient map \mathcal{C}'_T can be written as the following composition

$$\mathcal{C}'_T = \mathcal{C}_T \circ \mathcal{R}^c, \quad (13)$$

where the map $\mathcal{R}^c : \mathbb{R}^{2n+2} \supset \mathcal{D} \rightarrow \mathbb{R}^{2n+2}$ is the reparametrisation $\mathcal{R}^c(\theta) = (a_1, \dots, a_n, b_1, \dots, b_n, b_w, d)$ defined by (4); and \mathcal{C}_T is the coefficient map associated with the TF

$$T(s, \theta_{a,b}) = \sum_{i=1}^n \frac{b_i}{s + a_i} + \frac{b_w}{s} + d, \quad (14)$$

where $\theta_{a,b} = (a_1, \dots, a_n, b_1, \dots, b_n, b_w, d) \in \mathbb{R}^{2n+2}$. By Lemma 1 (for $m = n + 1$ and $a_{n+1} = 0$) the map \mathcal{C}_T is many-to-one; and \mathcal{R}^c is a one-to-one map with an inverse

$$R_\infty = d, \quad C_w = \frac{1}{b_w}, \quad R_i = \frac{b_i}{a_i}, \quad C_i = \frac{1}{b_i}, \quad i = 1, \dots, n.$$

The map \mathcal{C}'_T is many-to-one, since it is a composition of a one-to-one with many-to-one map. Thus for $n > 1$, the model structure $\mathcal{M}_{RC}(n)$ is locally identifiable.

Part (c). Finally, the identifiability equation (9) under the condition (12) admits a unique solution, which concludes part (c). \square

Remark 2: The same procedure is applicable to the discrete time model. The Euler's first order approximation is the simplest approximation. Its identifiability analysis is easier because the coefficients of the discrete time TF equals the number of parameters. However, it might lead to numerical instability. If higher order approximations are applied, the challenge remains to prove whether there is a finite-to-one maps between the discrete time model and parameters.

IV. SIMULATIONS

Consider a 6-element Randles circuit with $R_\infty, C_w, R_i, C_i, i = 1, 2$. In this section, accuracy of the estimation in the presence of DC-offset, noise-free and noisy data,

subject to random initial guess of estimations is studied. First the informative data set used in the simulations and the way it is generated are described. More details are provided in references [33], [45]–[47].

A. Generation of informative data set

A data set is informative if the input is persistently exciting. A persistently exciting input adequately excites all modes of the system. In linear systems, the order of the system determines the order of persistent excitation. The order of a persistent excitation equals the number of coefficients of the monic TF that need to be identified, (see Theorem 13.1. in [33]). The monic TF of the 6-element Randles circuit is

$$H(s) = \frac{f_3 s^3 + f_2 s^2 + f_1 s + f_0}{s^3 + g_2 s^2 + g_1 s + g_0} \quad (15)$$

with unknown coefficients to be identified. Therefore, the necessary order of the persistently exciting input is 7. In the frequency domain, this means that the spectrum of the excitation input should have at least 7 nonzero points. This simulation focuses on multi-sine excitation signals which are widely employed in electrochemical impedance spectroscopy (EIS) techniques, [3], [4], [48]. The same procedure can be applied to other inputs. The multi-sine signal is given by

$$u(t) = \sum_{j=1}^l m_j \cos(\omega_j t + \phi_j), \quad (16)$$

where l represents the number of sinusoids, and m_j, ω_j and $\phi_j \in [-\pi, \pi)$ denote the magnitude, frequency in radians per second and phase in radians, respectively. The spectrum of the multi-sine signal is given by

$$\Phi_u(\omega) = 2\pi \sum_{j=1}^l \frac{m_j^2}{4} [\delta(\omega - \omega_j) + \delta(\omega + \omega_j)], \quad (17)$$

where $\delta(\omega)$ is the delta function or impulse at frequency ω_j . The spectrum of each sinusoid signal contains two nonzero points, therefore 4 sinusoid signals are enough to generate the informative data set for the 6-element Randles circuit model.

The magnitudes m_j , frequencies ω_j and phases ϕ_j are arbitrary real values. Specific applications might impose additional constraints. For instance, in EIS techniques, the magnitude of the input signal may vary depending on the size of the energy storage system. If m_j 's are equal, the Schroeder phase choice is suggested to reduce the Crest factor [33], [49]. The frequencies could be equally or logarithmically spread over the frequency band $\omega_{\min} \leq \omega \leq \omega_{\max}$. The values of ω_{\min} and ω_{\max} depend on the system dynamics.

Remark 3: Depending on the application and testing facilities, we may need to use the battery as a load or a power supply only. In such a case, the battery excitation current is superimposed on a known DC offset to make sure that the battery current flows through one direction,

(see examples in [3] and [48]). The mean value of the multi-sine signal might not also be exactly zero. Thus, there might be a DC offset to the data. It is typically recommended to remove the DC offset in system identification. However, because the dynamic of the Warburg term is at low frequencies, it might be appropriate to keep the DC-offset. In this work, we study the effect of DC-offset to the estimation.

B. The results discussion

The following operating point is arbitrarily selected [4]:

$$\begin{aligned} R_\infty &= 0.05 \, \Omega, \quad R_1 = 0.2 \, \Omega, \quad C_1 = 0.3 \, \text{F} \\ R_2 &= 0.4 \, \Omega, \quad C_2 = 0.6 \, \text{F}, \quad C_w = 300 \, \text{F} \end{aligned}$$

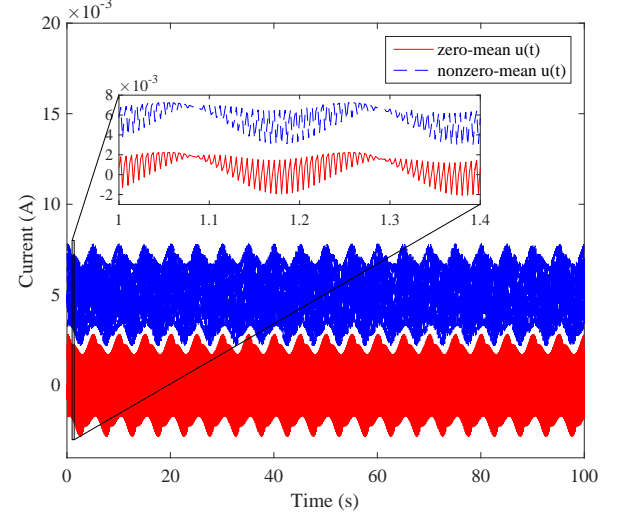
The multi-sine excitation signal is generated by using (16) with $l = 4$, $m_j = 10^{-3}$ for $j = 1, \dots, 4$, $f_{\min} = 0.2$ Hz, $f_{\max} = 500$ Hz and Schroeder phase with ϕ_1 randomly chosen at -0.95 . The mean value of the multi-sine signal is 1.9747×10^{-8} . In order to study the effect of the zero-mean data, this value is subtracted from the multi-sine signal. The crest factor of the zero-mean excitation signal is 1.999.

In order to study the effect of the nonzero-mean data, the original multi-sine signal, (i.e., with mean value of 1.9747×10^{-8}) is used. However, because its mean value is very small, the multi-sine signal is also superimposed on additional DC offsets to make the comparison between zero- and nonzero-mean data significant. As mentioned earlier, DC offset is used in applications where the battery current must flow through one direction only. Two DC offsets 0.005 A and 0.5 A, were chosen randomly, (five and five hundreds times the magnitude of the sinusoidal signals m_j , $j = 1, \dots, 4$). The associated crest factors of the nonzero-mean excitation signals are 0.544 (for the signal with DC=0.005) and 0.0057 (for the signal with DC=0.5).

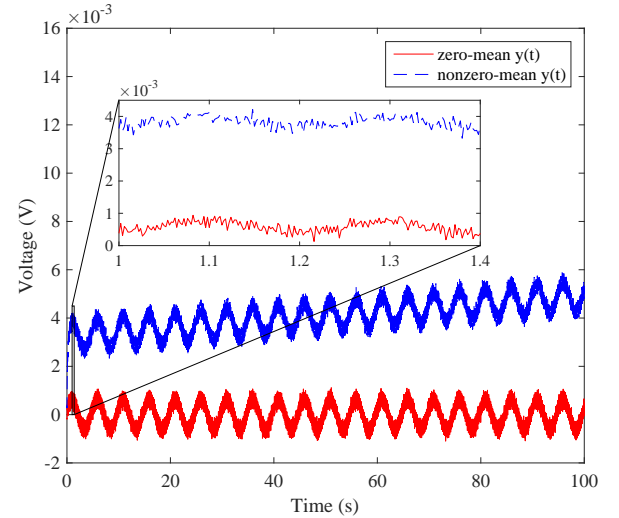
The voltage response is computed using the model in (2). In order to study the noise effect on the estimation accuracy, a zero-mean noise with standard deviation $\sigma = 10^{-4}$ is added to the output voltage $y(t)$. The signal to noise ratio is $\frac{10^{-3}}{10^{-4}} = 10$.

Figure 2 shows the zero-mean and nonzero-mean noisy data. To be readily visible, only the nonzero-mean data with DC offset 0.005 A are shown.

Given the true values, the smallest time constant is $\tau_{\min} = R_1 C_1 = 0.06$ s. The sampling time should be several times larger than $1/\tau_{\min}$. In this simulation, the sampling frequency is chosen at $f_s = 500$ Hz, which is 16.6 times greater than the inverse of the minimum time constant. The test duration should typically be several times larger than the maximum time constant, which is $\tau_{\max} = R_\infty C_w = 15$ s. In [47], 6 to 8 times τ_{\max} is suggested, however, this might vary in different applications. In this simulation, a test duration of $t_d = 100$ s is applied. The continuous-time TF (15) is identified using Matlab's system identification toolbox [50]. Estimation results from zero-mean, nonzero-mean, noise-free and noisy data are compared together. The circuit parameters are calculated



(a) Excitation input $u(t)$.



(b) Associated output $y(t)$.

Fig. 2. The zero- and nonzero-mean multi-sine excitation signals and associated noisy outputs for $R_\infty = 0.05 \, \Omega$, $R_1 = 0.2 \, \Omega$, $C_1 = 0.3 \, \text{F}$, $R_2 = 0.4 \, \Omega$, $C_2 = 0.6 \, \text{F}$, and $C_w = 300 \, \text{F}$. The voltage response, Figure 2(b), is computed using the model (2). The output noise is zero-mean random value with standard deviation $\sigma = 10^{-4}$. To be readily visible, only the nonzero-mean data with DC offset 0.005 A are shown.

directly from the coefficients of the TF using the formulas shown in Table III and discussed later. In order to study the consistency of results, each test is repeated 100 times, every run with a random initial guess of parameters. The roots of the denominator must be positive real numbers. Those estimations, which lead to complex or negative poles for the TF, or to $C_w > 1000$ or to $C_i > 10$, $i = 1, 2$, are considered outliers and discarded from the analysis.

The relative mean error, e_r is defined as follows:

$$e_r = 100 \times \left| \frac{\text{true value} - \text{mean of estimations}}{\text{true value}} \right| \%. \quad (18)$$

Tables I and II show the average of results over 100 times

running the simulation by using noise-free, noisy, zero- and nonzero-mean data.

C. The effect of DC-offset on estimations

By comparing the zero-mean and nonzero-mean data in Table I, it is seen that estimations by using the zero-mean noise-free data converge with average e_r 's less than 10% for R_i , C_i , $i = 1, 2$ and for C_w . The largest e_r is 10.137% for R_∞ . However, estimations by using the nonzero-mean noise-free data lead to significantly larger relative errors. Only relative estimation error of the Warburg term C_w is reduced by using the nonzero-mean noise-free data.

The use of the nonzero-mean noise-free data will also reduce the standard deviation of C_w , but will increase the standard deviation of R_∞ , R_i , C_i , $i = 1, 2$.

The number of outliers will also increase by using the nonzero-mean data.

The comparison of estimations by using the zero-mean data and nonzero-mean noisy data in Table II confirms the same results.

Figures 3 and 4 show the histograms of accepted estimations by using zero- and nonzero- mean noisy data, over 100 times running the simulation. Because of page limitation, the results of nonzero-mean data with DC offset 0.005 A are only shown. The figures confirm that standard deviation of estimations using nonzero-mean data is very large, which dramatically deteriorate the estimation accuracy. The nonzero-mean data only improves the estimation error and standard deviation of C_w . Therefore, there is a trade-off between the estimation accuracy of C_w and other parameters by using the zero- and nonzero- mean data. However, it is noted that the average of the relative error of C_w is less than 2%, with zero-mean data, which might be enough for some applications.

D. The effect of the value of DC-offset on estimations

The estimation results by using the nonzero-mean data with DC offsets 0.005 A and 0.5 A are compared together. In the noise-free case (Table I), it is seen that, the larger the DC offset, the more the outliers. Table II shows the same result with noisy data. However, no consistent increment or decrement is seen on the relative error and standard deviation of estimations.

E. The effect of noise on estimations

By comparing estimation results from the zero-mean noise-free and the zero-mean noisy data from Tables I and II, it is seen that relative errors of estimations do not change consistently (it might increase or decrease). For instance, e_r of R_∞ increases, but e_r of C_1 decreases when the zero-mean noisy data is used. Similarly, no consistent variation is seen on the relative error of estimations from the nonzero-mean noise-free and noisy data for both DC-offsets.

When zero-mean data is used, results show that standard deviations of estimations increase with the noise.

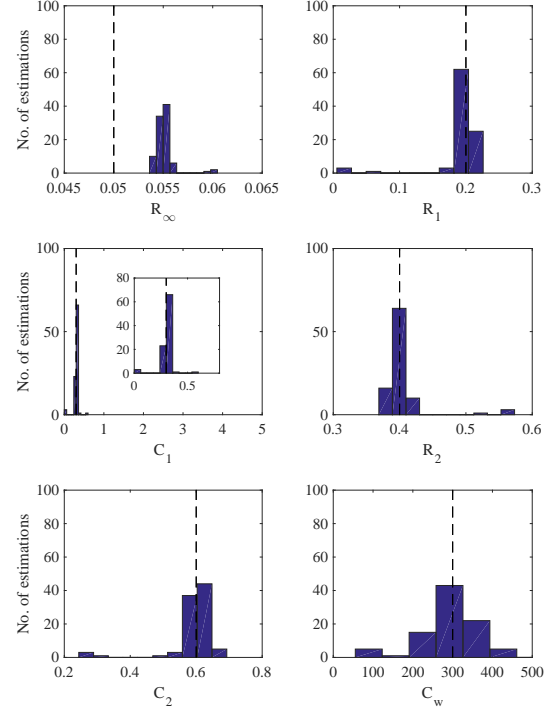


Fig. 3. Histograms of accepted estimations in 100 runs from zero-mean noisy data.

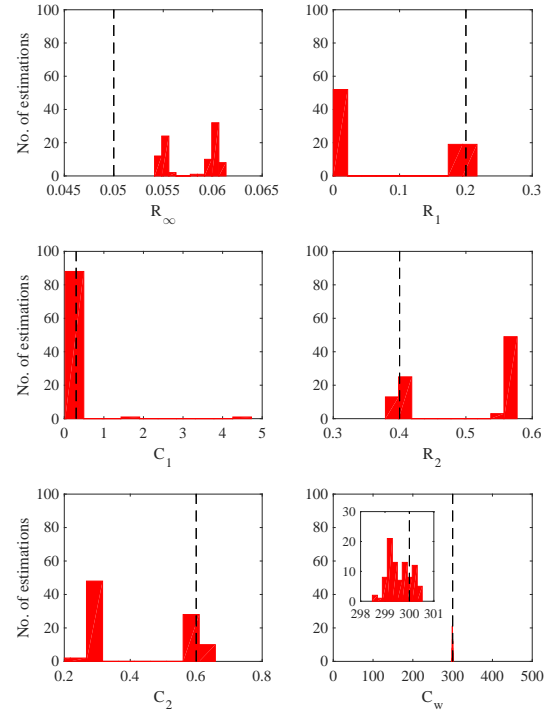


Fig. 4. Histograms of accepted estimations in 100 runs from nonzero-mean noisy data.

TABLE I
ESTIMATION RESULTS OF NOISE-FREE DATA.

	Parameter True Value	R_∞ 0.05	R_1 0.2	C_1 0.3	R_2 0.4	C_2 0.6	C_w 300
zero-mean data (7 outliers)	mean	0.055	0.193	0.299	0.402	0.595	294.785
	st.d.	0.001	0.028	0.044	0.025	0.052	35.395
	e_r	10.137	3.696	0.506	0.519	0.862	1.738
Data with DC offset 0.005 A (10 outliers)	mean	0.058	0.087	0.184	0.502	0.408	299.560
	st.d.	0.003	0.092	0.124	0.086	0.162	0.368
	e_r	15.847	56.750	38.829	25.444	32.075	0.147
Data with DC offset 0.5 A (59 outliers)	mean	0.062	0.062	0.357	0.461	0.635	299.258
	st.d.	0.019	0.108	1.067	0.122	1.284	1.638
	e_r	23.576	68.993	19.101	15.239	5.818	0.247

TABLE II
ESTIMATION RESULTS OF NOISY DATA.

	Parameter True Value	R_∞ 0.05	R_1 0.2	C_1 0.3	R_2 0.4	C_2 0.6	C_w 300
zero-mean data (6 outliers)	mean	0.055	0.190	0.299	0.404	0.590	301.552
	st.d.	0.001	0.037	0.062	0.035	0.075	93.493
	e_r	10.309	4.981	0.264	1.081	1.642	0.517
Data with DC offset 0.005 A (10 outliers)	mean	0.058	0.088	0.246	0.500	0.408	299.584
	st.d.	0.003	0.093	0.513	0.086	0.167	0.470
	e_r	16.052	56.120	18.051	24.891	31.991	0.139
Data with DC offset 0.5 A (57 outliers)	mean	0.058	0.074	0.422	0.462	0.521	299.664
	st.d.	0.006	0.086	0.909	0.083	0.635	4.672
	e_r	14.938	62.787	40.777	15.390	13.103	0.112

For the DC-offset 0.005 A, this increment is small. By increasing the DC-offset to 0.5 A, standard deviations of estimations become inconsistent. Analytical proofs of these observation require more research.

As concluding remarks, the majority of estimations (including the relative estimation error of C_w) by using the zero-mean data results in average errors less than 10%. The estimation of Warburg term can further be improved by using the nonzero-mean data, however, accuracy and standard deviation of estimations of other parameters are reduced and increased, respectively.

The largest standard deviation (specially with the zero-mean data) is for C_w . This could be because of the pure integrator associated with C_w , which appears in the TF, which might require some modifications of the data set, [51]. For instance, a methodology has been proposed in [36] that removes the integral term by modifying the input signal as $i_{\text{modified}}(t) = \int i(t)dt$.

F. Calculating the coefficients of $R - R||C - R||C - C$ circuit

Here we show how to compute the parameters of the 6-element Randles circuit. Using (5), the circuit's TF is:

$$H(s) = \frac{f_3 s^3 + f_2 s^2 + f_1 s + f_0}{s^3 + g_2 s^2 + g_1 s + g_0}$$

The relationships between the coefficients and the circuit parameters are given by:

$$\begin{aligned} f_3 &= d, \quad f_2 = b_1 + b_2 + b_w + (a_1 + a_2)d \\ f_1 &= a_2 b_1 + a_1 b_2 + (a_1 + a_2)b_w + a_1 a_2 d, \quad f_0 = a_1 a_2 b_w \\ g_2 &= a_1 + a_2, \quad g_1 = a_1 a_2, \quad g_0 = 0 \end{aligned} \quad (19)$$

where the parameters a_i , b_i , b_w and d are as defined in (4).

Because the circuit has an integrator, the identification method should be set up such that a pole of the denominator is fixed at $s = 0$. The identification software typically allows to fix a number of poles and zeros at certain values, [50]. Using the first equation of (19) and (4), R_∞ is given by:

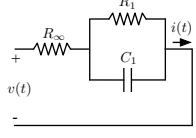
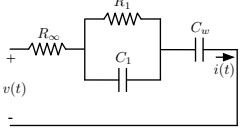
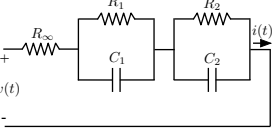
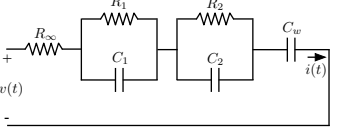
$$R_\infty = f_3$$

The roots of $s^3 + g_2 s^2 + g_1 s + g_0 = 0$ are a_1 and a_2 , and the one that has been fixed at $s = 0$. By using the condition (12), select the smallest root as a_2 , and the remaining root as a_1 . From (4), the circuit's time constants are obtained as follows:

$$\tau_i = \frac{1}{a_i} \text{ for } i = 1, 2.$$

From (19) and (12), b_1 , b_2 and b_w are obtained by solving

TABLE III
THE COEFFICIENTS OF FOUR WIDELY USED RANDES CIRCUIT MODELS.

			
Estimated TF: $H(s) = \frac{f_1 s + f_0}{s + g_0}$	Estimated TF: $H(s) = \frac{f_2 s^2 + f_1 s + f_0}{s^2 + g_1 s + g_0}$ Set up to identify a pole at $s = 0$	Estimated TF: $H(s) = \frac{f_2 s^2 + f_1 s + f_0}{s^2 + g_1 s + g_0}$	Estimated TF: $H(s) = \frac{f_3 s^3 + f_2 s^2 + f_1 s + f_0}{s^3 + g_2 s^2 + g_1 s + g_0}$ Set up to identify a pole at $s = 0$
$R_\infty = f_1$ $a_1 = g_0$ $\tau_1 = \frac{1}{a_1}$	$R_\infty = f_2$ $\text{roots}([1 \ g_1 \ g_0]) \Rightarrow a_1, 0$ $\tau_1 = \frac{1}{a_1}$ $AX = B$ $A = \begin{bmatrix} 1 & 1 \\ 0 & a_1 \end{bmatrix}$ $B = \begin{bmatrix} f_1 - a_1 f_2 \\ f_0 \end{bmatrix}$ $b_1 = f_0 - a_1 f_1$ $C_1 = \frac{1}{b_1}$ $R_1 = \frac{\tau_1}{C_1}$	$R_\infty = f_2$ $\text{roots}([1 \ g_1 \ g_0]) \Rightarrow a_1, a_2$ choose $a_2 < a_1$ $\tau_i = \frac{1}{a_i}$ $AX = B$ $A = \begin{bmatrix} 1 & 1 \\ a_2 & a_1 \end{bmatrix}$ $B = \begin{bmatrix} f_1 - (a_1 + a_2)f_2 \\ f_0 - a_1 a_2 f_2 \end{bmatrix}$ $X = \begin{bmatrix} b_1 & b_2 \end{bmatrix}^\top$ $C_i = \frac{1}{b_i}$ $R_i = \frac{\tau_i}{C_i}, \ i = 1, 2$	$R_\infty = f_3$ $\text{roots}([1 \ g_2 \ g_1 \ g_0]) \Rightarrow a_2, a_1, 0$ choose $a_2 < a_1$ $\tau_i = \frac{1}{a_i}$ $AX = B$ $A = \begin{bmatrix} 1 & 1 & 1 \\ a_2 & a_1 & a_1 + a_2 \\ 0 & 0 & a_1 a_2 \end{bmatrix}$ $B = \begin{bmatrix} f_2 - (a_1 + a_2)f_3 \\ f_1 - a_1 a_2 f_3 \\ f_0 \end{bmatrix}$ $X = \begin{bmatrix} b_1 & b_2 & b_w \end{bmatrix}^\top$ $C_i = \frac{1}{b_i}$ $C_w = \frac{1}{b_w}$ $R_i = \frac{\tau_i}{C_i}, \ i = 1, 2$

the following set of equations for X :

$$\begin{bmatrix} 1 & 1 & 1 \\ a_2 & a_1 & a_1 + a_2 \\ 0 & 0 & a_1 a_2 \end{bmatrix} X = \begin{bmatrix} f_2 - (a_1 + a_2)f_3 \\ f_1 - a_1 a_2 f_3 \\ f_0 \end{bmatrix}$$

where,

$$X = \begin{bmatrix} b_1 & b_2 & b_w \end{bmatrix}^\top$$

Other parameters of the circuit are subsequently obtained as:

$$C_w = \frac{1}{b_w}, \quad C_i = \frac{1}{b_i}, \quad R_i = \frac{\tau_i}{C_i}, \quad i = 1, 2.$$

The parameters of different topologies can simply be calculated using the same approach. Table III provides formulas for four widely used Randles models.

V. CONCLUSIONS

We showed that the generalised Randles circuit model is locally identifiable and the model structure becomes

globally identifiable if an ordering through the circuit is assumed. The results were confirmed through extensive simulations. Finally, explicit formulas for the coefficients of widely used Randles circuits were presented. The effects of the DC-offset and noise were studied extensively. The existing trade-off between the estimations of Warburg term and other parameters by using the zero- and nonzero-mean data were fully discussed.

ACKNOWLEDGEMENTS

This work was funded by the University of Oxford EPSRC Impact Acceleration Account Technology Fund Awards EP/K503769/1 and EP/K036157/1. The authors would like to thank the anonymous reviewers and the editor for their fruitful comments that significantly improved the paper. We would like also to extend our thanks to Ross Drummond, Stephen Duncan, Xinfan Lin and Shi Zhao for their feedback on the first version of this work.

REFERENCES

- [1] J. Randles, "Kinetics of rapid electrode reactions," *Discuss. Faraday Soc.*, vol. 1, pp. 11–19, 1947.
- [2] C. Rahn and C.-Y. Wang, *Battery Systems Engineering*. John Wiley Sons, 2013.
- [3] S. M. M. Alavi, C. R. Birkel, and D. A. Howey, "Time-domain fitting of battery electrochemical impedance models," *Journal of Power Sources*, vol. 288, pp. 345–352, 2015.
- [4] E. Barsoukov and J. R. Macdonald, *Impedance Spectroscopy: Theory, Experiment, and Applications*, 2nd ed. John Wiley & Sons, 2005.
- [5] S. Buller, M. Thele, R. W. A. A. De Doncker, and E. Karden, "Impedance-based simulation models of supercapacitors and li-ion batteries for power electronic applications," *IEEE Transactions on Industry Applications*, vol. 41, pp. 742–747, 2005.
- [6] D. Andre, M. Meiler, K. Steiner, C. Wimmer, T. Soczka-Guth, and D. U. Sauer, "Characterization of high-power lithium-ion batteries by electrochemical impedance spectroscopy. I. Experimental investigation," *Journal of Power Sources*, vol. 196, pp. 5334–5341, 2011.
- [7] Y. Hu, S. Yurkovich, Y. Guezennec, and B. J. Yurkovich, "Electro-thermal battery model identification for automotive applications," *Journal of Power Sources*, vol. 196, pp. 449–457, 2011.
- [8] C. Birkel and D. Howey, "Model identification and parameter estimation for LiFePO₄ batteries," *Hybrid and Electric Vehicles Conference 2013 (HEVC 2013)*, pp. 2.1–2.1, 2013.
- [9] H. Rahimi-Eichi, F. Baronti, and M. Y. Chow, "Online adaptive parameter identification and state-of-charge coestimation for lithium-polymer battery cells," *IEEE Transactions on Industrial Electronics*, vol. 61, pp. 2053–2061, 2014.
- [10] V. Mihajlovic, B. Grundlehner, R. Vullers, and J. Penders, "Wearable, wireless eeg solutions in daily life applications: What are we missing?" *IEEE Journal of Biomedical and Health Informatics*, vol. 19, pp. 6–21, 2015.
- [11] S. Bugenhagen, A. Cowley Jr., and D. Beard, "Baroreceptor dynamics and their relationship to afferent fiber type and hypertension," *Physiological Genomics*, vol. 42, pp. 23–41, 2010.
- [12] A. Mahdi, J. Sturdy, T. Ottesen, and M. Olufsen, "Modeling the afferent dynamics of the baroreflex control system," *PLoS Computational Biology*, vol. 9, p. e10033384, 2013.
- [13] G. Mader, M. Olufsen, and A. Mahdi, "Modeling cerebral blood flow velocity during orthostatic stress," *Annals of biomedical engineering*, pp. 1–11, 2014, doi:10.1007/s10439-014-1220-4.
- [14] J. Lee, J. Lee, O. Nam, J. Kim, B. H. Cho, H.-S. Yun, S.-S. Choi, K. Kim, J. Kim, and S. Jun, "Modeling and Real Time Estimation of Lumped Equivalent Circuit Model of a Lithium Ion Battery," *12th International Power Electronics and Motion Control Conference*, pp. 1536 – 1540, 2006.
- [15] N. Moubayed, J. Kouta, A. El-Ali, H. Dernayka, and R. Outbib, "Parameter identification of the lead-acid battery model," *2008 33rd IEEE Photovoltaic Specialists Conference*, pp. 1–6, 2008.
- [16] J. Jang and J. Yoo, "Equivalent circuit evaluation method of lithium polymer battery using bode plot and numerical analysis," *IEEE Transactions on Energy Conversion*, vol. 26, pp. 290–298, 2011.
- [17] S. Jiang, "A Parameter Identification Method for a Battery Equivalent Circuit Model," *SAE Technical Paper*, 2011.
- [18] B. Pattipati, C. Sankavaram, and K. R. Pattipati, "System identification and estimation framework for pivotal automotive battery management system characteristics," *IEEE Transactions on Systems, Man and Cybernetics Part C: Applications and Reviews*, vol. 41, pp. 869–884, 2011.
- [19] A. Rahmoun and H. Biehl, "Modelling of Li-ion batteries using equivalent circuit diagrams," *PRZEGLAD ELEKTROTECHNICZNY*, vol. 2, pp. 152–156, 2012.
- [20] R. Al-Nazer and V. Cattin, "A new optimization algorithm for a Li-Ion battery equivalent electrical circuit identification," *9th International Conference of Modeling, Optimization and Simulation*, 2012.
- [21] A. Raue, C. Kreutz, T. Maiwald, J. Bachmann, M. Schilling, U. Klingmüller, and J. Timmer, "Structural and practical identifiability analysis of partially observed dynamical models by exploiting the profile likelihood," *Bioinformatics*, vol. 25, pp. 1923–1929, 2009.
- [22] C. Cobelli and J. J. DiStefano, "Parameter and structural identifiability concepts and ambiguities: a critical review and analysis," *The American journal of physiology*, vol. 239, pp. R7–R24, 1980.
- [23] R. Bellman and K. Åström, "On structural identifiability," *Mathematical Biosciences*, vol. 7, pp. 329–339, 1970.
- [24] H. Pohjanpalo, "System identifiability based on the power series expansion of the solution," *Mathematical Biosciences*, vol. 41, pp. 21–33, 1978.
- [25] M. J. Chappell, K. R. Godfrey, and S. Vajda, "Global identifiability of the parameters of nonlinear systems with specified inputs: A comparison of methods," *Mathematical Biosciences*, vol. 102, pp. 41–73, 1990.
- [26] S. Vajda, K. R. Godfrey, and H. Rabitz, "Similarity transformation approach to identifiability analysis of nonlinear compartmental models," *Mathematical biosciences*, vol. 93, pp. 217–248, 1989.
- [27] F. Anstett, G. Bloch, G. Millérioux, and L. Denis-Vidal, "Identifiability of discrete-time nonlinear systems: The local state isomorphism approach," *Automatica*, vol. 44, pp. 2884–2889, 2008.
- [28] N. Meshkat and S. Sullivant, "Identifiable reparametrizations of linear compartment models," *Journal of Symbolic Computation*, vol. 63, pp. 46–67, 2014.
- [29] A. Mahdi, N. Meshkat, and S. Sullivant, "Structural identifiability of viscoelastic mechanical systems," *PLoS ONE*, vol. 9, 2014.
- [30] K. Glover and J. Willems, "Parametrizations of linear dynamical systems: Canonical forms and identifiability," *IEEE Transactions on Automatic Control*, vol. AC-19, no. 6, pp. 640 – 646, 1974.
- [31] J. Distefano, "On the relationships between structural identifiability and the controllability, observability properties," *IEEE Transactions on Automatic Control*, vol. 22, p. 652, 1977.
- [32] J. M. Van Den Hof, "Structural identifiability of linear compartmental systems," *IEEE Transactions on Automatic Control*, vol. 43, pp. 800–818, 1998.
- [33] L. Ljung, *System Identification Theory for the User*. PTR Prentice Hall Upper Saddle River NJ, 1987.
- [34] L. Ljung and T. Glad, "On global identifiability for arbitrary model parametrizations," *Automatica*, vol. 30, pp. 265–276, 1994.
- [35] S. Audoly, G. Bellu, L. D'Angiò, M. P. Saccomani, and C. Cobelli, "Global identifiability of nonlinear models of biological systems," *IEEE Transactions on Biomedical Engineering*, vol. 48, pp. 55–65, 2001.
- [36] M. Sitterly, L. Y. Wang, G. G. Yin, and C. Wang, "Enhanced identification of battery models for real-time battery management," *IEEE Transactions on Sustainable Energy*, vol. 2, pp. 300–308, 2011.
- [37] M. Rausch, S. Streif, C. Pankiewicz, and R. Findeisen, "Non-linear observability and identifiability of single cells in battery packs," *IEEE International Conference on Control Applications (CCA)*, pp. 401–406, 2013.
- [38] A. P. Schmidt, M. Bitzer, A. W. Imre, and L. Guzzella, "Experiment-driven electrochemical modeling and systematic parameterization for a lithium-ion battery cell," *Journal of Power Sources*, vol. 195, pp. 5071–5080, 2010.
- [39] J. C. Forman, S. J. Moura, J. L. Stein, and H. K. Fathy, "Genetic identification and fisher identifiability analysis of the Doyle-Fuller-Newman model from experimental cycling of a LiFePO₄ cell," *Journal of Power Sources*, vol. 210, pp. 263–275, 2012.
- [40] S. J. Moura, N. A. Chaturvedi, and M. Krstić, "Adaptive Partial Differential Equation Observer for Battery State-of-Charge/State-of-Health Estimation Via an Electrochemical Model," *Journal of Dynamic Systems, Measurement, and Control*, vol. 136, p. 011015, 2013.
- [41] A. M. D'Amato, J. C. Forman, T. Ersal, A. Ali, J. L. Stein, H. Peng, and D. S. Bernstein, "Noninvasive battery-health diagnostics using retrospective-cost identification of inaccessible subsystems," *ASME 2012 5th Annual Dynamic Systems and Control Conference Joint with the JSME 2012 11th Motion and Vibration Conference*, pp. 1–9, 2012.
- [42] A. Sharma and H. Fathy, "Fisher identifiability analysis for a periodically-excited equivalent-circuit lithium-ion battery model," *American Control Conference (ACC)*, pp. 274–280, 2014.

- [43] M. Rothenberger, J. Anstrom, S. Brennan, and H. Fathy, "Maximizing Parameter Identifiability of an Equivalent-Circuit Battery Model Using Optimal Periodic Input Shaping," *ASME 2014 Dynamic Systems and Control Conference*, pp. 1–10, 2014.
- [44] R. L. M. Peeters and B. Hanzon, "Symbolic computation of Fisher information matrices for parametrized state-space systems," *Automatica*, vol. 35, pp. 1059–1071, 1999.
- [45] T. Söderström and P. Stoica, *System identification*. Prentice-Hall, 1989.
- [46] J. P. Norton, *An introduction to identification*. Academic Press, 1986.
- [47] Y. Zhu, *Multivariable System Identification For Process Control*. Elsevier, 2001.
- [48] D. A. Howey, P. D. Mitcheson, V. Yufit, G. J. Offer, and N. P. Brandon, "Online measurement of battery impedance using motor controller excitation," *IEEE Transactions on Vehicular Technology*, vol. 63, pp. 2557–2566, 2014.
- [49] M. Schroeder, "Synthesis of low-peak-factor signals and binary sequences with low autocorrelation," *IEEE Transactions on Information Theory*, vol. 16, pp. 85 – 89, 1970.
- [50] L. Ljung, *System Identification Toolbox For Use with MATLAB*. The MathWorks, Inc., 1988.
- [51] B. D. O. Anderson and J. B. Moore, *Optimal Filtering*. Dover Publications, 2005.